JTTEE5 14:511-517
DOI: 10.1361/105996305X76531
1059-9630/$19.00 © ASM International

In Situ Measurement System for Deformation and Solidification Phenomena of Yttria-Stabilized Zirconia Droplets Impinging on Quartz Glass Substrate under Plasma-Spraying Conditions

Kentaro Shinoda, Yoichi Kojima, and Toyonobu Yoshida

(Submitted September 24, 2004; in revised form January 24, 2005)

The authors have developed an in situ measurement system for precise one-to-one correlation between splat morphology and thermal history during particle impingement on a temperature-controlled substrate inside an airtight chamber under plasma-spraying conditions. The system has made it possible to collect about 10 single particles successively within a 10 s time frame, and to correlate exactly the relationship between the size, the temperature, and the impacting velocity of each droplet, and the morphology of the splats. The most striking finding is that a part of the yttria-stabilized zirconia (YSZ) droplets may be actually in supercooled condition before impinging, although a marked difference was not found in the splat morphology. In addition, as secondary results, we could evaluate the viscosity, μ, of YSZ, and the thermal contact resistance between YSZ splat and the quartz glass substrate as μ [Pa · s] = 0.0037 exp (6110/*T*) and 3×10^{-6}-4×10^{-5} m^2 K/W, respectively.

Keywords diagnostics and control, influence of cooling properties, influence of process parameters, influence of spray parameters, RF induction plasma spraying, splat cooling, thermal barrier coating topcoats

1. Introduction

The application fields of thermal plasma spraying are now expanding to many new technological fields, such as thermal barrier coatings (TBCs) (Ref 1) and solid oxide fuel cells (Ref 2), due to their high productivity and cost effectiveness. Recently, some projects have started to investigate next-generation TBCs for new applications of thermal plasma-spraying technology (Ref 3), which may demand even nano-level-designed microstructures. To achieve this, basic studies to investigate the elemental process of thermal plasma spraying are highly desired. However, the spraying process is too complicated to be analyzed or measured simply, because it is characterized by successive and/or parallel processes made up of injection, acceleration, melting, deformation, solidification, and adhesion of the particles, and each process is usually completed within a very short time on the order of microseconds to milliseconds. On the measurements conducted to examine an in-flight process, many excellent articles have been published in the last decade (Ref 4-6), but there have been only a few papers relating to the deposition process (Ref 7-10). On the other hand, outstanding numerical analysis and simulations relating to the deformation and solidification process of sprayed particles have been developed rapidly (Ref 11-18). Unfortunately, however, most of these simulations have to assume thermal contact resistance between the splat and the substrate as a fitting parameter, although it cannot be applied simply in cases where the temperature gap exceeds 2000 K. Therefore, it is clear that a complementary approach between in situ measurement and numerical simulation is needed to understand the fundamental process in the spraying, and experimental approaches have been highly anticipated at this stage. Moreau et al. (Ref 19) measured the temperature of TiC particles impacting on the stainless steel substrate under direct current (dc) plasma spraying, and showed the feasibility of infrared monitoring of the temperature of a plasma-sprayed particle at the moment of impact and immediately after. Vardelle et al. (Ref 7) also measured the particle size, velocity, and surface temperature impinging on the substrate under dc plasma spraying. Gougeon and Moreau (Ref 9) developed a simultaneous independent measurement system for splat diameter and cooling time during impact on a substrate of plasma-sprayed molybdenum particles, in which they measured the shading area of the laser beam during spreading. However, the correlation between the splat morphology and the measurement results is not always sufficient in their system. Therefore, in the present research, the authors developed an in situ measurement system to individualize each single-sprayed particle and to monitor the impact of the particle successively on the temperature-controlled substrate in an airtight chamber.

The original version of this paper was published as part of the DVS Proceedings: "Thermal Spray Solutions: Advances in Technology and Application," International Thermal Spray Conference, Osaka, Japan, 10-12 May 2004, CD-Rom, DVS-Verlag GmbH, Düsseldorf, Germany.

Kentaro Shinoda, Yoichi Kojima, and **Toyonobu Yoshida,** The University of Tokyo, Department of Materials Engineering, Graduate School of Engineering, 7-3-1, Hongo, Bunkyo-ku, Tokyo 113-8656 Japan. Contact e-mail: shinoda@plasma.t.u-tokyo.ac.jp.

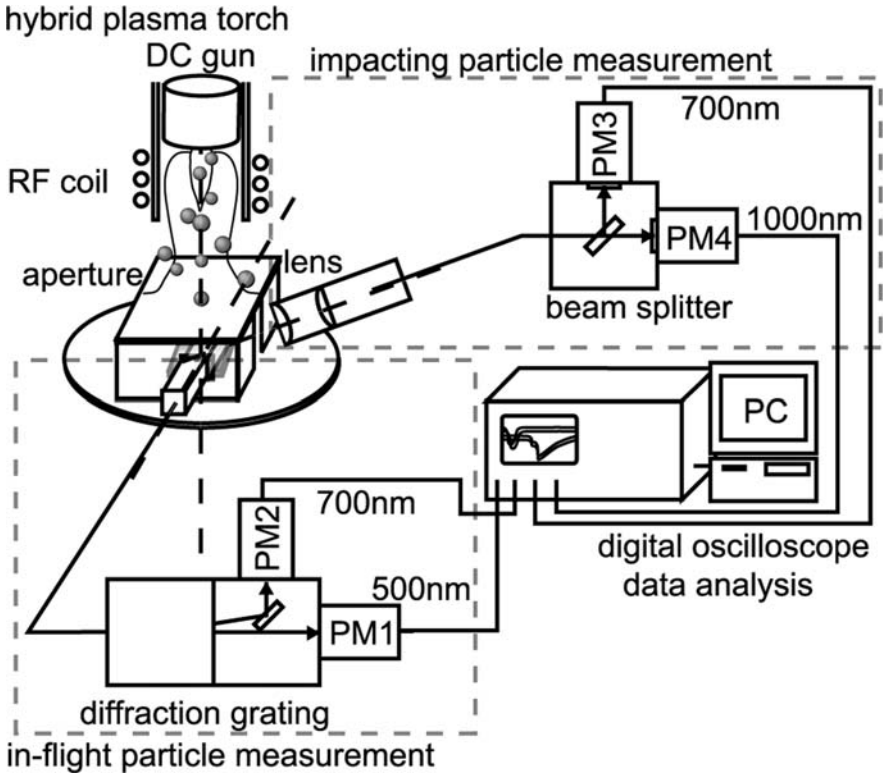

Fig. 1 Schematic diagram of the in situ measurement system, which consists of five different parts: dc-rf hybrid plasma torch; single-particle collection part; in-flight particle measurement system; impacting particle measurement system; and data analysis facility

2. Experimental

The newly developed in situ measurement system is shown schematically in Fig. 1. The system consists mainly of a hybrid plasma-spraying system, a single particle collection apparatus, two sets of emission detectors, and a data storage apparatus. The hybrid plasma-spraying system consists of a radio frequency (rf) power supply of 4 MHz-60 kW, a dc power supply of 10 kW, a dc-rf hybrid plasma torch, and an airtight chamber. This made it possible to measure the deformation and solidification process under a wide variety of conditions such as: a wide range of an yttria-stabilized zirconia (YSZ) powder particle size up to 100 μm, particle velocities ranging from 20 to 70 m/s, and various atmospheres as well as a wide pressure range. Figure 2 shows a schematic view of a cross section of the part of the system that collects single particles successively. Essentially, a set of boron nitride (BN) plates with an orifice was used to regulate the number of particles so that only one or two particles can reach the substrate per second. The diameter of the orifice of the first (upper side) plate and that of the second (lower side) plate were 1.5 mm and 500 μm, and their distances from the substrate were 30 and 7 mm, respectively. The first was set to limit the number of in-flight particles to avoid clogging the second orifice. A collimator with a slit of 600 μm in height and 800 μm in width was set immediately under the second aperture to measure the velocity and temperature of the in-flight particle. The diameter of the second orifice was smaller than the slit width of the collimator, so the collimator was able to detect all of the particles that pass through the second orifice. In addition, the substrate holder was designed to be movable horizontally with a speed up to 1 mm/s to avoid overlapping of the splats. The first aperture served also as a radiation-heating device for the substrate. It prevented rapid heating of the substrate by the plasma flame, but could be heated up to 2000 K, and consequently had the capability to heat the substrate up to 700 K. Figure 3 shows an example of the temperature increase at the quartz substrate as a function of time after opening the shutter. The temperature, measured by a thermocouple, increased gradually up to 600 K and remained constant during the experiment. Because only 10 s was needed to carry out a whole measurement, temperature variation during the experiment was expected to be within a few degrees kelvin and to be negligible, even if the experiment was conducted before the substrate reached a steady state with respect to the temperature. The temperature variation as a function of time shown in Fig. 3 suggests the usefulness of the heating device for controlling the substrate temperature.

Two optical systems were used to detect the thermal emission from a particle. One was used to measure the surface temperature and velocity of the in-flight particle immediately before the particle impinged, and connected to the collimator described above, utilizing the method developed by Sakuta and Boulos (Ref 5). The authors selected 500 and 700 nm wavelengths for the temperature measurement. The detected signal itself works as a trigger for the record of a sequence measurement for the event of particle flattening. The other system was connected to the emission condenser, which consisted of two optical lenses with the focal lengths of 40 and 70 mm. This condenser focused at an angle of 20° on the substrate, and its viewing field on the

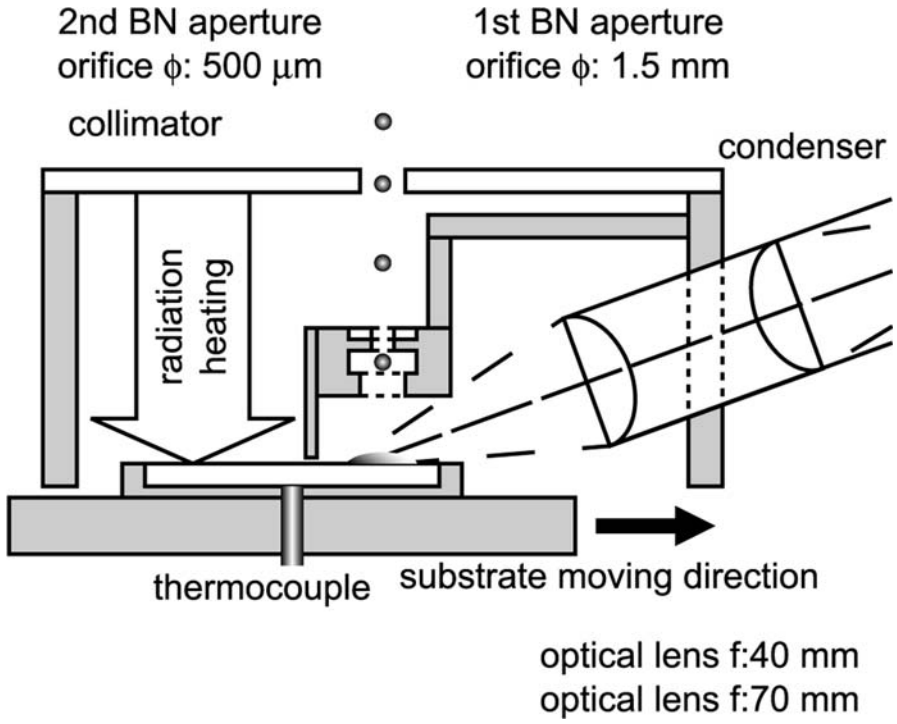

Fig. 2 Schematic view of the collection part for single particles, which can collect single sprayed particles and individualize each particle by two boron nitride apertures. The upper aperture also functions as a radiation heater.

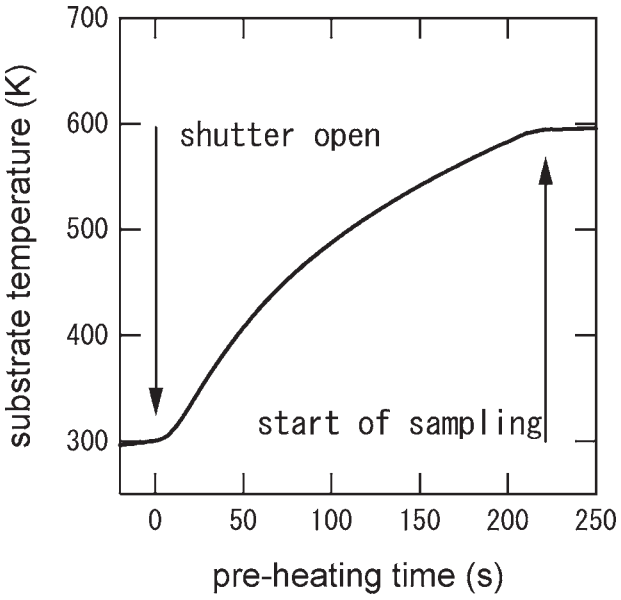

Fig. 3 Substrate temperature history during preheating by the boron nitride aperture

substrate was an ellipse of 1.7 × 5 mm. The detected light was divided into reflection and transmission lights by a beam splitter, and then was filtered by 10 nm width narrow band-pass filters of 700 and 1000 nm, respectively. The photomultipliers used here were: R1104 for 500 nm; R2228 for 700 nm for in-flight particle measurement; R943-02 for 700 nm; and R3310-02 for 1000 nm for impact (all made by Hamamatsu Photonics, K.K., Shizuoka, Japan). The digital oscilloscope (TDS-754D, Tektronix, Japan, Ltd., Tokyo, Japan) has four-channel monitors with an 8-bit vertical resolution, namely, a maximum time resolution of 1 ns per sample, and can memorize 50,000 addresses/channel. It also has an important function in that it can share one buffer during one experiment, which makes it possible to collect single particles successively. The data collected by the digital oscilloscope were sent to a personal computer via gerenal purpose-interface bus (GP-IB). The droplet diameter was calculated from the volume of the deposited splat. The volume was measured precisely with a three-dimensional laser microscope (VK-8500, Keyence Corporation, Osaka, Japan) that can measure the three-dimensional morphology, which was also used to examine the backside of splats.

Table 1 Experimental conditions

Parameters	Settings
Internal diameter of the dc torch, mm	6
Dc Ar gas flow rate, slm	10
Dc current, A	400
Internal diameter of the rf torch, mm	40
Rf tangential Ar gas flow rate, slm	10
Rf radial Ar gas flow rate, slm	30
Rf radial hydrogen gas flow rate, slm	5
Rf input, kW	50
Powder carrier gas flow rate, slm	2
Powder feeding rate, g, min	0.6
Stand-off distance, cm	8

Table 1 shows the spraying conditions. The powders are injected into the dc plasma jet at an angle of 30° from the torch axis

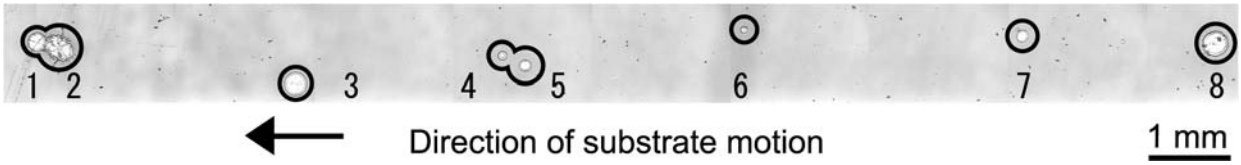

Fig. 4 Image of the laser microscope of the collected YSZ splats on the quartz substrate

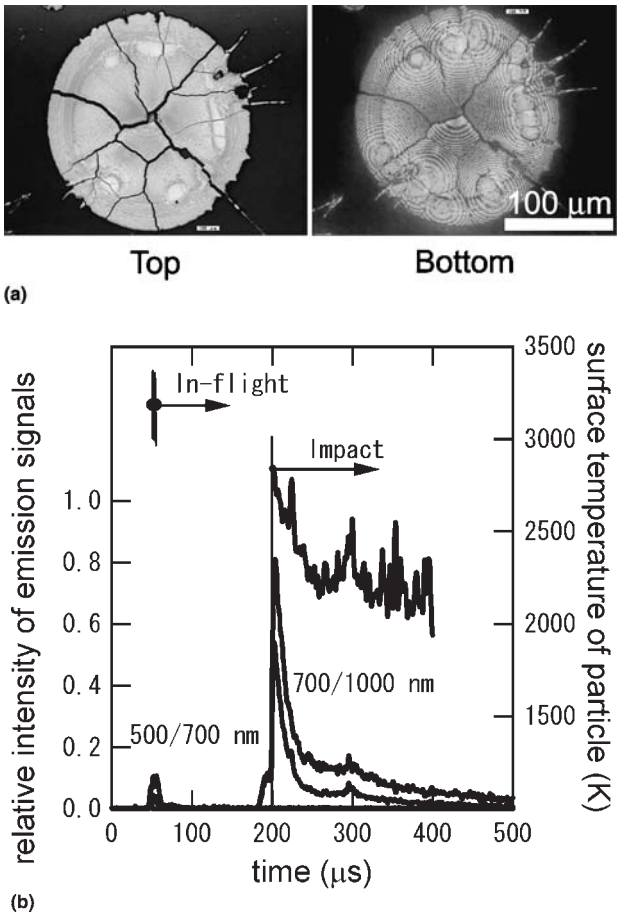

Fig. 5 (a) Images obtained by the laser microscope of an example YSZ splat from both top and bottom sides. (b) Example waveforms obtained by two temperature measurement systems corresponding to the splat shown in (a)

through a tube with a 2 mm internal diameter passed through the inside of the anode. The authors have repeated the following experiment and collected splats. Fused and crushed 8YSZ powder with a particle size distribution ranging from 63 to 88 μm was used. The 8%H_2-Ar atmospheric hybrid plasma was adapted to spray the powder onto a quartz substrate moving at 1 mm/s. The substrate measured 20 mm long by 10 mm wide by 0.7 mm thick, and its surface roughness was 0.04 μm. The stand-off distance was set to 8 cm. The powder-feeding rate was adjusted below 0.6 g/min to limit the number of particles impinging on the substrate. The substrate temperature was set at approximately 600 K to obtain disk-shaped splat (Ref 20). The sampling rate was set to a 0.1 μs interval, and the sampling points were 5000 for each channel for one splat.

3. Results

Figure 4 shows an image of the YSZ splats on the quartz substrate obtained in one trial. The arrow indicates the direction of substrate motion during spraying. It was observed that eight splats were collected successively in a line on the substrate. The time intervals between these splats were 0.274, 2.236, 1.777, 0.282, 1.784, 3.292, and 1.769 s from left to right, in order.

Figure 5(a) shows an example of the collected splats. The left- and right-hand pictures show the top view and bottom view of the splat. The diameter of the splat, D, and that of the droplet derived, d, were 212 and 77 μm, respectively, and the flattening degree, D/d, was hence 2.8 in this case. Interference stripes can be observed from both the top and bottom sides. From the bottom side view, it can be observed that the heterogeneous nucleations of solidification actually occurred randomly along the periphery. Figure 5(b) shows the corresponding waveforms to the splat shown in Fig. 5(a) obtained by the two optical systems, which were smoothed by the Savitzky-Golay algorithm (Ref 21). They revealed that the particle-impingement velocity, V, was 49 m/s, the surface temperature of the particle just at impact, T_{im}, was approximately 2900 K, the deformation time, t_d, was 4.0 μs, and the cooling rate, C_R, was 1.2×10^7 K/s. The t_d is defined here as the period from the detection of the 700/1000 nm emission signals to the intensity maximum, and the cooling rate is defined as the gradient of the temperature history when the intensities of the emission signals begin to decrease. Plateau or recalescence was not observed clearly in this study; thus, the solidification time could not be evaluated precisely.

Figure 6 shows the relationship among the V, T_{im}, and d under hybrid plasma spraying. The range of V was dispersed from 30 to 80 m/s, and that of the T was dispersed from 2500 to 3800 K. The distribution of the d was from 30 to 90 μm. The T_{im} decreased with the increase of the d, and there was no obvious relationship between the V and other parameters.

Most of the collected splats corresponding to the particles in Fig. 6 were disk-shaped, but some large splats showed fingering at the periphery. Figure 7 shows the D/d, t_d, and C_R as a function of the d. Open and filled circles indicate the droplets that impinged on the substrate at temperatures above and below the melting point of zirconia, 3000 K, respectively. The D/d had a moderate peak in the d of 40 to 70 μm, and the average of D/d was 3.0. The t_d was varied from 3.3 to 5.6 μs and tended to increase with the increase of the d. There was no significant difference in the D/d and t_d between the droplets impinging at temperatures above and below 3000 K. The cooling rate was on the order of 4×10^6 to 1×10^8 K/s, and there was no relation with the V or T_{im}, but there was a clear relation with the d. It should also be noted that the dispersions both in the t_d and C_R of the droplets below 3000 K were larger than those of droplets over 3000 K,

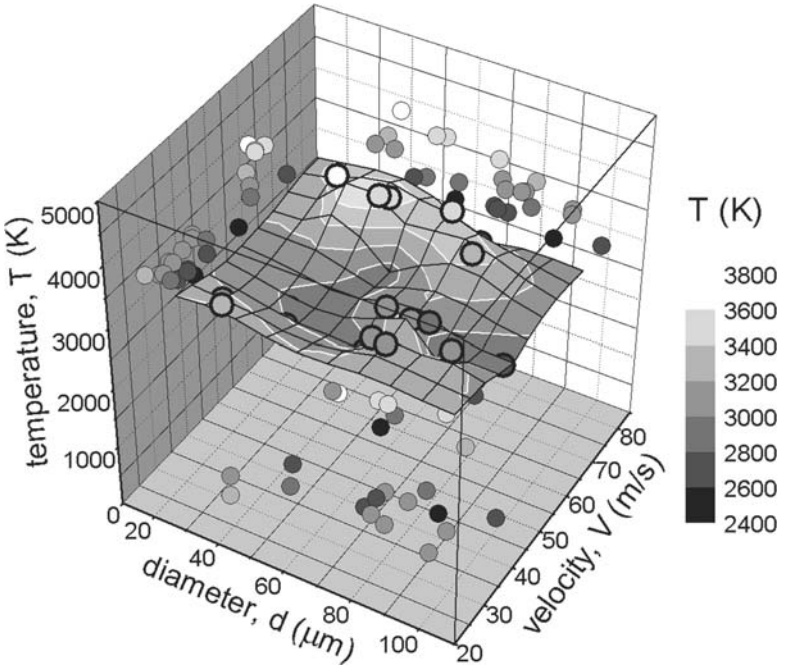

Fig. 6 Relationship among droplet diameter, impact velocity, and impact temperature

although there was no obvious difference in the D/d. This was probably due to the supercooling effects, which will be discussed in the next section. Another interesting subsidiary result derived from the measurement relates to the heat transfer coefficient, h, between the zirconia splat and the quartz substrate, which was derived from the correlation: $C_R = h(T_{im} - T_{sub})/(\rho \cdot C_p \cdot L)$, where T_{sub} is the substrate temperature, 600 K, C_p is the specific heat of zirconia, 713 J/kg K (Ref 22), ρ is the density of zirconia, 5700 kg/m^3 (Ref 8), and L is the measured splat thickness. Under the simplified assumption, the derived values ranging from 3×10^4 to 3×10^5 W/m^2 K were the lower limit of h, and the inverse of h, 3×10^{-6} to 4×10^{-5} m^2 K/W, were the larger limit of thermal contact resistance, R_C. Vardelle et al. (Ref 8) reported that the value of the R_C varies between 10^{-7} and 10^{-8} m^2 K/W in the case of the stainless steel substrate. One of the reasons for this may be due to the different substrate materials, but the difference is considered to be mainly caused by the difference in the impact velocity, namely, 30 to 70 m/s for the case of hybrid plasma spraying and 150 to 230 m/s for the case of dc plasma spraying.

4. Discussion

The authors successfully sampled 10 single splats that were successively deposited in a row on the substrate within 10 s. This is very useful for the statistical evaluation of the fundamental process of particle impingement and also make it possible to evaluate the particle size precisely. Although the size and velocity estimation was conducted very precisely, the accuracy of the temperature measurements needed to be improved via consideration of the fact that the Biot number of zirconia droplets under plasma spraying is often over unity and that zirconia is a semi-transparent material, as Dombrovsky and Ignatiev have indicated (Ref 23). On the other hand, focusing on the temperature history during droplet spreading, the authors could not observe either an obvious plateau or recalescence in the experiments. However, it would still be unwise to conclude that recalescence does not occur under the conditions, because the temperature distribution inside the splat during deformation is clearly nonuniform and also because the background noise was serious in the initial stage of the deformation.

Among the experiments, there were some droplets impacting at low temperatures near 2500 K. They also adhered to the substrate, formed disk-shaped splats, and did not have solidified shells, which indicate that the solidification did not occur before impact. Although each droplet is semitransparent and the temperature gradient inside the particle cannot be negligible in large zirconia powders, it can be said that there existed a supercooled droplet. Nevertheless, the surface morphologies and the flattening degree of those splats did not show a big difference with those of superheated droplets. This finding, namely, the degree of supercooling in the droplet, and the lack of any effect on spreading and splat formation, is somewhat surprising, but is the most interesting finding and merits much further investigation because no one has measured such supercooled droplets under spraying conditions.

From a modeling approach, on the other hand, the lack of knowledge of the high-temperature properties of zirconia has clearly prevented the development of a realistic simulation. In reality, there are only a few articles referring to viscosity. For example, Fantassi et al. (Ref 24) assumed a constant value of 0.04 Pa · s, and Vardelle et al. (Ref 8) used the equation $\mu[\text{Pa} \cdot \text{s}] = 0.1 \exp(-2.95 + 5993/T)$, which was based on the analogy with the temperature dependence of alumina viscosity. Hence, the authors have estimated the viscosity of zirconia, μ, by substituting

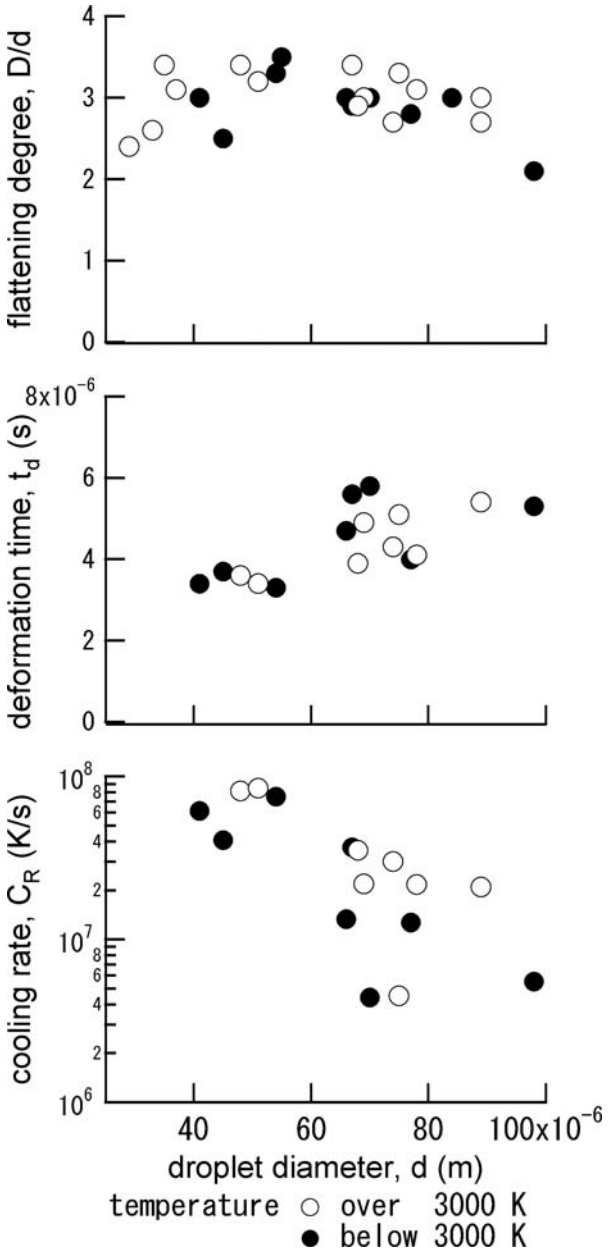

Fig. 7 Flattening degree, deformation time, and cooling rate as a function of droplet diameter

the results into the model: $D/d = 0.83\mathrm{Re}^{0.2}$ (Ref 25). Each value could be fitted by the Arrhenius-type equation $\mu[\mathrm{Pa} \cdot \mathrm{s}] = 0.0037 \exp(6100/T)$, revealing 0.028 Pa · s at 3000 K, as shown in Fig. 8. The viscosities of the alumina reported in the literature (Ref 26-31) are also shown for the purpose of comparison. The viscosity of zirconia does not increase rapidly with the increase of supercooling, which was different from what had been expected. This low viscosity in the supercooling region will be the main reason why supercooled droplets can show a similar degree of flattening as that of superheated droplets. The kinematic viscosities at melting points of zirconia (3000 K) and alumina (2328 K) are 4.9×10^{-6} and 1.5×10^{-5} m^2/s (Ref 31), respectively. The value of zirconia is approximately three times smaller than that

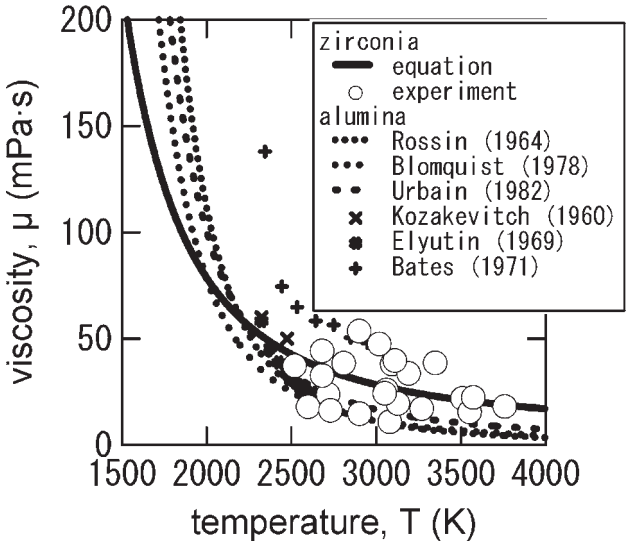

Fig. 8 Estimated viscosity of zirconia. Viscosities of alumina are adopted from Kozakevitch (Ref 26), Rossin et al.(Ref 27), Elyutin et al. (Ref 28), Bates et al. (Ref 29), Blomquist (Ref 30), and Urbain (Ref 31).

of alumina, which suggests that zirconia particles may flatten better than alumina particles once they are fully melted. Note that the activation energy for zirconia viscosity was derived as 51 kJ/mol, which is much lower than the value of 247 kJ/mol proposed by Sudreau and Cognet (Ref 32), and was rather close to the values 87 and 68 kJ/mol that were estimated by Grosse (Ref 33) and Hirai (Ref 34) relationships for metallic alloys, respectively. The derived value of μ is only a rough estimation; nevertheless, the fact that we can deduce even the unknown viscosity of zirconia clearly reveals the power of our approach.

5. Conclusions

The main points of this study are:

- An in situ measurement system has been developed that is able to individualize each single sprayed particle, and to correlate the splat morphology with the impact velocity and the thermal history of each particle during the impact on a substrate.
- The one-to-one correspondence between the splat and the emission signals made it possible to evaluate the effects of droplet size precisely.
- There existed the particles considered to be in supercooling states before impacting under plasma-spraying conditions.
- Fundamental values of the flattening process such as the viscosity of zirconia, and thermal contact resistance were evaluated through the measurement.

Acknowledgments

The present research is financed by the Japan Society for the Promotion of Science (No. 12305048) and is supported in part by a Grant for 21st Century Center of Excellence (COE) Program "Human-Friendly Materials based on Chemistry" from the

Ministry of Education, Culture, Sports, Science, and Technology of Japan. The authors thank Mr. Ryuta Takenoshita for his help concerning the data acquisition system and also thank Mr. Yoshio Hasegawa for his help concerning the experimental setup.

References

1. N.P. Padture, M. Gell, and E.H. Jordan, Thermal Barrier Coatings for Gas-Turbine Engine Applications, *Science,* Vol 296 (No. 5566), 2002, p 280-284
2. F. Gitzhofer, M. Boulos, J. Heberlein, R. Henne, T. Ishigaki, and T. Yoshida, Integrated Fabrication Processes for Solid-Oxide Fuel Cells Using Thermal Plasma Spray Technology, *MRS Bull.,* Vol 25 (No. 7), 2000, p 38-42
3. T. Yoshida, Some Issues for the Development of Spraying Technology, *Mater. Japan,* Vol 40 (No. 4), 2001, p 322-325 (in Japanese)
4. J.R. Fincke, C.L. Jeffery, and S.B. Englert, In-Flight Measurement of Particle-Size and Temperature, *J. Phys. E: Sci. Instrum.,* Vol 21 (No. 4), 1988, p 367-370
5. T. Sakuta and M.I. Boulos, Novel-Approach for Particle-Velocity and Size Measurement under Plasma Conditions, *Rev. Sci. Instrum.,* Vol 59 (No. 2), 1988, p 285-291
6. J.R. Fincke, D.C. Haggard, and W.D. Swank, Particle Temperature Measurement in the Thermal Spray Process, *J. Therm. Spray Technol.,* Vol 10 (No. 2), 2001, p 255-266
7. M. Vardelle, A. Vardelle, P. Fauchais, and C. Moreau, Pyrometer System for Monitoring the Particle Impact on a Substrate during a Plasma Spray Process, *Meas. Sci. Technol.,* Vol 5 (No. 3), 1994, p 205-212
8. M. Vardelle, A. Vardelle, A.C. Leger, P. Fauchais, and D. Gobin, Influence of Particle Parameters at Impact on Splat Formation and Solidification in Plasma Spraying Processes, *J. Therm. Spray Technol.,* Vol 4 (No. 1), 1995, p 50-58
9. P. Gougeon and C. Moreau, Simultaneous Independent Measurement of Splat Diameter and Cooling Time during Impact on a Substrate of Plasma-Sprayed Molybdenum Particles, *J. Therm. Spray Technol.,* Vol 10 (No. 1), 2001, p 76-82
10. C. Moreau, P. Cielo, and M. Lamontagne, Flattening and Solidification of Thermally Sprayed Particles, *J. Therm. Spray Technol.,* Vol 1 (No. 4), 1992, p 317-324
11. G. Trapaga and J. Szekely, Mathematical-Modeling of the Isothermal Impingement of Liquid Droplets in Spraying Processes, *Metall. Trans. B,* Vol 22 (No. 6), 1991, p 901-914
12. M. Pasandideh-Fard, Y.M. Qiao, S. Chandra, and J. Mostaghimi, Capillary Effects during Droplet Impact on a Solid Surface, *Phys. Fluids,* Vol 8 (No. 3), 1996, p 650-659
13. M. Bussmann, S. Chandra, and J. Mostaghimi, Modeling the Splash of a Droplet Impacting a Solid Surface, *Phys. Fluids,* Vol 12 (No. 12), 2000, p 3121-3132
14. Y.K. Chae, J. Mostaghimi, and T. Yoshida, Deformation and Solidification Process of a Super-Cooled Droplet Impacting on the Substrate Under Plasma Spraying Conditions, *Sci. Technol. Adv. Mater.,* Vol 1 (No. 3), 2000, p 147-156
15. J.P. Delplanque and R.H. Rangel, An Improved Model for Droplet Solidification on a Flat Surface, *J. Mater. Sci.,* Vol 32 (No. 6), 1997, p 1519-1530
16. V.V. Sobolev, J.M. Guilemany, and A.J. Martin, Investigation of Droplet Flattening during Thermal Spraying, *Surf. Coat. Technol.,* Vol 89, 1997, p 82-89
17. Y.P. Wan, H. Zhang, X.Y. Jiang, S. Sampath, and V. Prasad, Role of Solidification, Substrate Temperature and Reynolds Number on Droplet Spreading in Thermal Spray Deposition: Measurements and Modeling, *Trans. ASME,* Vol 123, 2001, p 382-389
18. H. Zhang, X.Y. Wang, L.L. Zheng, and X.Y. Jiang, Studies of Splat Molphology and Rapid Solidification during Thermal Spraying, *Int. J. Heat Mass Transfer,* Vol 44, 2001, p 4579-4592
19. C. Moreau, P. Cielo, M. Lamontagne, S. Dallaire, and M. Vardelle, Impacting Particle Temperature Monitoring during Plasma Spray Deposition, *Meas. Sci. Technol.,* Vol 1 (No. 8), 1990, p 807-814
20. K. Shinoda, P. Han, and T. Yoshida, "The Microstructure of YSZ Splats Deposited by Hybrid Plasma Spraying," *Proceedings of the 15th International Symposium on Plasma Chemistry* (Orleans, France), Vol 4. A. Bouchoule, et al., Ed., 2001, p 2661-2666
21. A. Savitzky and M.J.E. Golay, Smoothing and Differentiation of Data by Simplified Least Squares Procedures, *Anal. Chem.,* Vol 36 (No. 8), 1964, p 1627-1639
22. M.W.J. Chase, Ed., NIST-JANAF Thermochemical Tables, 4th ed., Journal of Physical and Chemical Reference Data, Vol 9, American Chemical Society and American Institute of Physics for the National Institute of Standards and Technology, 1998
23. L.A. Dombrovsky and M.B. Ignatiev, An Estimate of the Temperature of Semitransparent Oxide Particles in Thermal Spraying, *Heat Transfer Eng.,* Vol 24 (No. 2), 2003, p 60-68
24. S. Fantassi, M. Vardelle, A. Vardelle, and P. Fauchais, Influence of the Velocity of Plasma-Sprayed Particles on Splat Formation, *J. Thermal Spray Technol.,* Vol 2 (No. 4), 1993, p 379-384
25. T. Yoshida, T. Okada, H. Hamatani, and H. Kumaoka, Integrated Fabrication Process for Solid Oxide Fuel Cells Using Novel Plasma Spraying, *Plasma Sources Sci. Techol.,* Vol 1 (No. 3), 1992, p 195-201
26. P. Kozakevitch, Viscosite et elements structuraux des aluminosilicates fondus: laitiers CaO-Al2O3-SiO2 entre 1600 et 2100 C, *Rev. Met.,* Vol 57, 1960, p 149-160 (in French)
27. R. Rossin, J. Bersan, and G. Urbain, Etude de la viscosite de laitiers liquides appartenant au systeme ternaire: SiO2-Al2O3-CaO, *Rev. Hautes Temper. Refract.,* Vol 1, 1964, p 159-170 (in French)
28. V.P. Elyutin, V.I. Kostikov, B.S. Mitin, and Y.A. Nagibin, Measurement of Viscosity of Aluminum Oxide, *Zh. Fiz. Khim.,* Vol 43, 1969, p 579-583 (in Russian)
29. J.L. Bates, C.E. McNeilly, and J.J. Rasmussen, Properties of Molten Ceramics, *Ceramics in Severe Environments: Proceedings, Materials Science Research,* W.W. Kriegel and H.I. Palmour, Ed., Plenum Press, 1971, p 11-26
30. R.A. Blomquist, J.K. Fink, and L. Leibowitz, Viscosity of Molten Alumina, *Am. Ceram. Soc. Bull.,* Vol 57 (No. 5), 1978, p 522
31. G. Urbain, Viscosite de l'alumine liquide (Viscosity of Liquid Alumina), *Rev. Int. Hautes Temp. Refract.,* Vol 19 (No. 1), 1982, p 55-57 (in French)
32. F. Sudreau and G. Cognet, Corium Viscosity Modelling Above Liquidus Temperature, *Nucl. Eng. Des.,* Vol 178, 1997, p 269-277
33. A.V. Grosse, The Empirical Relationship between the Activation Energy Viscosity of Liquid Metals and Their Melting Points, *J. Inorg. Nucl. Chem.,* Vol 255, p 317-318
34. M. Hirai, Estimation of Viscosities of Liquid Alloys, *ISIJ Int.,* Vol 33 (No. 2), p 251-258